Received: 30 November 2023 | Accepted: 30 November 2023

DOI: 10.1002/asna.20230170

Astronomische Nachrichten

PROCEEDING

Fulfilling modern astrophysical observations and lattice QCD constraints based on a nonlocal NJL model with 3D form factor

G. A. Contrera[1,2] | **J. P. Carlomagno**[1,2] | **A. G. Grunfeld**[1,3]

[1]CONICET, Godoy Cruz 2290 (C1425FQB) CABA, Argentina

[2]IFLP, CONICET - Departamento de Física, Facultad de Ciencias Exactas, Universidad Nacional de La Plata, La Plata, Argentina

[3]Physics Department, Comisión Nacional de Energía Atómica (C.N.E.A), Buenos Aires, Argentina

Correspondence
G. A. Contrera, Departamento de Física, Facultad de Ciencias Exactas, Universidad Nacional de La PLata, C.C. 67, (1900), La Plata, Argentina.
Email: contrera@fisica.unlp.edu.ar

Funding information
Consejo Nacional de Investigaciones Científicas y Técnicas, Grant/Award Number: PIP11220210100150CO; Facultad de Ciencias Exactas, Universidad Nacional de La Plata, Grant/Award Number: X960; Fondo para la Investigación Científica y Tecnológica, Grant/Award Numbers: PICT19-00792, PICT20-01847

Abstract

In the present work, we employ a nonlocal Nambu–Jona–Lasinio (NJL) model with a Gaussian form factor that is dependent on the spatial components of the momentum (3D-FF). Focusing on the temperature-baryon chemical potential plane, we investigate some aspects of the phase diagram. Initially, we propose an assumption that the range of interactions in momentum space may be modified by temperature, allowing us to obtain the critical temperature values based on lattice QCD (LQCD) predictions. Subsequently, we consider this model within a hybrid framework to examine the effects of temperature, together with neutrino trapping, in compact object configurations.

KEYWORDS

Nambu–Jona–Lasinio models, nonperturbative QCD, quark matter

1 | INTRODUCTION

The study of the QCD phase diagram, which continues to attract significant attention, shows the different phases of strongly interacting matter according to temperature and baryon chemical potential (Fukushima & Hatsuda 2011). In environments of extraordinary temperature and density, like those witnessed in the early universe or within neutron stars (NSs; Lattimer & Prakash 2016; Page & Reddy 2006), nuclear matter shifts between different phases, including the quark-gluon plasma, hadronic matter, and the color superconducting phases.

However, at low energies, QCD becomes nonperturbative, and effective models emerge as essential tools for describing the relevant phenomena in that regime (Hatsuda & Kunihiro 1994; Klevansky 1992; Vogl & Weise 1991). On the one hand, at low temperatures and high densities or baryonic chemical potential, effective models should be capable of representing and predicting the phenomena occurring within compact stars. Furthermore, for nearly zero baryonic chemical potential,

effective models should align with the predictions of lattice QCD (LQCD; Ding et al. 2015; Karsch 2002).

In previous work (Contrera et al. 2022), we extensively analyzed the outcomes of a nonlocal chiral quark model including color superconductivity and vector repulsive interactions, at zero temperature. The objective was to use the resultant equation of state (EOS) for quark matter (QM) along with a hadronic EOS to comprehensively depict the properties of cold, deleptonized NSs within a hybrid framework. We identified the optimal parameters of the QM model that satisfy maximum mass, radii, and tidal deformability observational constraints (Abbott & e. a 2018; Ayriyan et al. 2021; Hebeler et al. 2013; Miller & e. a 2021).

With that background, in this study, we expand our previous model considering finite temperature, while meeting two essential criteria: compatibility with LQCD and consistency with multimessenger astrophysical observations.

First of all, we aim to explore the higher-temperature region of the phase diagram, corresponding to vanishing baryonic chemical potential, while ensuring compatibility with the critical temperature described by LQCD (Borsanyi et al. 2020; Karsch & Laermann 2004), where the chiral symmetry restoration and the confinement/deconfinement transition take place.

The local NJL model (Nambu & Jona-Lasinio 1961a,b) lacks confinement. However, by incorporating the Polyakov loop potential (Fukushima & Skokov 2017; Polyakov 1978), it becomes feasible to describe both transitions. It is worth emphasizing that the inclusion of the Polyakov-loop leads to the breakdown of the color SU(3) symmetry to SU(2). Consequently, the rotational invariance concerning the orientation choice of the 2SC gap under color neutrality constraints might be compromised (as pointed out in Gomez Dumm et al. (2008)). Consequently, the determination of the true minimum of the thermodynamic potential becomes a nontrivial task. We propose a simple approach to mimic color confinement and fit the chiral critical temperature to LQCD data. We parameterize the interaction range as a function of temperature, assuming that temperature can alter the range of interactions in momentum space.

Subsequently, to extend the study to finite temperature T and higher densities, we utilize the same parameters of the QM model from Contrera et al. (2022) to ensure the fulfillment of constraints relevant to the cold NS scenario. Incorporating T, we account for the trapped neutrinos in the compact star matter to examine their combined effects on the maximum mass and radii of the compact object configurations.

This work is structured as follows. In Section 2, we offer a succinct overview of the formalism. We incorporate the LQCD constraint to the critical temperature predicted by our model and we show the obtained phase diagrams. In Section 3, we present a study of hybrid compact object configurations at various temperatures, taking into account the neutrino chemical potential and the presence of electrons in the system. Finally, in Section 4, we outline our concluding remarks.

2 | FORMALISM AND NUMERICAL RESULTS

Here, we present the properties of QM using a nonlocal chiral quark model that includes interactions involving scalar and vector quark-antiquark pairs, as well as the scalar antitriplet of diquark interactions. The resulting pressure is

$$P_q = -\frac{(\overline{\sigma}^2 - \overline{\sigma}_0^2)}{2G_S} - \frac{\overline{\Delta}^2}{2G_D} + \frac{\overline{\omega}^2}{2G_V} + 2\int \frac{d^3\vec{p}}{(2\pi)^3}\,(\xi(\vec{p}) - \xi_0(\vec{p})), \tag{1}$$

with

$$\xi(\vec{p}) = \sum_{k,s,c} 2\left\{\epsilon_c^k/2 + T\,\ln\left[1 + e^{-\frac{\epsilon_c^k + s\;\delta\tilde{\mu}_c}{T}}\right]\right\} \tag{2}$$

and

$$\epsilon_c^{\pm} = \tilde{E}_c^{\pm}\sqrt{1 + \left[g(\vec{p})\overline{\Delta}(1-\delta_{bc})/\tilde{E}_c^{\pm}\right]^2} \tag{3}$$

where $\tilde{E}_c^{\pm} = E \pm \tilde{\mu}_c$ with $E^2 = \vec{p}^{\,2} + M^2(\vec{p})$ and $M(\vec{p}) = m_c + g(\vec{p})\overline{\sigma}$, $\epsilon = \sqrt{\vec{p}^2 + m_e^2}$ and $g(\vec{p})$ the form factor presented subsequently. The mean field values, $\overline{\sigma}$, and $\overline{\Delta}$ are obtained by solving a system of coupled gap equations, supplemented by a constraint equation for $\overline{\omega}$:

$$\frac{\partial\Omega^{MFA}}{\partial\overline{\sigma}} = 0\,, \quad \frac{\partial\Omega^{MFA}}{\partial\overline{\Delta}} = 0\,, \quad \frac{\partial\Omega^{MFA}}{\partial\overline{\omega}} = 0. \tag{4}$$

The solutions for the gap equations in the vacuum, at $T = \mu = 0$, are denoted with the subscript 0 and are included in the quark pressure P_q following the renormalization procedure described in Contrera et al. (2022), where a more complete description and details of the model can be found.

From the quarks pressure, we can easily derive several other important quantities. In particular, quark and lepton densities and the quark chiral condensate and chiral susceptibility (Contrera et al. 2022). By analyzing the last two order parameters of the theory, the phase diagram is obtained. In general, one can find regions in which the

chiral symmetry is either broken (χSB) or approximately restored, and phases in which the system remains either in an asymptotically free phase (NQM) or in a two-flavor superconducting phase (2SC).

When exploring the behavior of QM in NS cores, we must account for the simultaneous presence of electrons and the corresponding (anti)neutrinos. Thus, treating these leptons as a free relativistic Fermi gas, the total pressure of the QM plus leptons is given by $P = P_q + P_{lep}$, where the lepton pressure is defined as

$$P_{lep} = 2\,T \sum_{s=\pm} \int \frac{d^3\vec{p}}{(2\pi)^3} \ln\left[1 + e^{-\frac{\epsilon + s\,\mu_e}{T}}\right] + \left(\frac{\mu_{\nu_e}^4}{24\pi^2} + \frac{\mu_{\nu_e}^2\,T^2}{12} + \frac{7\pi^2\,T^4}{360}\right). \quad (5)$$

In addition, it is necessary to take into account that QM has to be in β-equilibrium with electrons through the β-decay reactions. Thus, we have an additional relation between fermion chemical potentials, namely,

$$\mu_{Q_q} = \mu_{uc} - \mu_{dc} = -\mu_e + \mu_{\nu_e} \quad (6)$$

for $c = r, g, b$, and e denotes electrons. As a consequence, the number of independent chemical potentials is reduced further. Finally, in the core of NSs, we also require the system to be electric and color charge neutral, then, the electron and color chemical potentials (μ_e and μ_8, respectively) get fixed by the condition that charge and color number densities vanish. In essence, in the context of QM in NSs, the values of $\overline{\Delta}$, $\overline{\sigma}$, $\overline{\omega}$, μ_e, and μ_8 can be determined for each combination of temperature T and baryonic chemical potential μ_B. In this study, we treat μ_{ν_e} as an input parameter, as explained in detail below. This determination involves solving Equation (4), along with additional constraints, such as chemical equilibrium, β-equilibrium, and electric and color charge neutrality. This comprehensive approach enables the establishment of the EOS for QM within the specific thermodynamic regime under consideration.

To fully specify the described nonlocal NJL model one has to fix, at $T = \mu_B = 0$, the model parameters as well as the instantaneous form factor $g(\vec{p})$ that characterize the nonlocal interactions between quarks in both channels $q\overline{q}$ and qq. As in Contrera et al. (2022), we consider a Gaussian form factor in momentum space,

$$g(\vec{p}) = \exp[-\vec{p}^{\,2}/\Lambda_0^2].$$

Fitting LQCD results of Burgio et al. (2012), in the Coulomb gauge, for the normalized quark effective mass $M(\vec{p})/M(0)$ (Contrera et al. 2022), we obtain $\Lambda_0 = 885.5$ MeV. Given the form factor functions, it is possible to set the model parameters to reproduce the observed meson phenomenology. Therefore, by requiring that the model reproduces the empirical values of the pion mass $m_\pi = 138$ MeV and the pion weak decay constant $f_\pi = 92.4$ MeV, it can be determined the remaining model parameters $m_c = 2.3$ MeV and $G_S = 9.9$ GeV^{-2}.

In the present QM model, the presence of 2SC color superconductivity at finite temperature leads to a clear color symmetry between red and green (we considered $\overline{\Delta}_5 = \overline{\Delta}_7 = 0$, $\overline{\Delta}_2 = \overline{\Delta}$). However, this symmetry contradicts the color gauge framework where the Polyakov loop takes on a diagonal representation (Abuki et al. 2009; Diakonov & Oswald 2004). Several studies (e.g., Blanquier (2017); Roessner et al. (2007); Gomez Dumm et al. (2008)) have integrated both effects in their respective diagonal gauges. However, it is essential to consider this approach as an approximation, as explained in the concluding section of Gomez Dumm et al. (2008).

Therefore, the standard mechanism for introducing color confinement cannot be applied in a NJL model with superconductivity. In addition, when the NJL is coupled to the Polyakov loop, the chiral critical temperature can be adjusted to LQCD results by the parameter T_0 that appears in the Polyakov effective potential $\mathcal{U}[T_0]$ (Pagura et al. 2012).

In this study, where a nonlocal NJL-like model with diquarks is considered, to mimic color confinement and be able to fit the chiral critical temperature at $\mu_B = 0$ to LQCD data, the range of the interaction Λ will be parameterized as a function that depends on the temperature and a free dimensionless parameter κ. In this way, we are assuming that the range of the interactions in momentum space can be modified by the temperature.

In our approach, performed in the mean-field approximation, the corrections due to interactions to the coupling constant should be provided by the loop diagrams coming from ring diagrams.

Since the range of the interactions in nonlocal models is controlled by the form factor in the quark currents, we propose, similar to what is found in QED,[1] a temperature dependence for the energy scale in our model, $\Lambda(T)$. As a first approximation, we propose a polynomial function in T as a thermal correction for the interaction range, namely

$$\Lambda(T) = \Lambda_0 \left(1 + \kappa \left(\frac{T}{\Lambda_0}\right)^2\right), \quad (7)$$

In addition to the prior suggestion, other functional forms have been considered, such as exponential and

[1] In QED, the loop contributions to the partition function generate dependence on the energy scale and temperature in the coupling constant of the theory (Kapusta & Gale 2011).

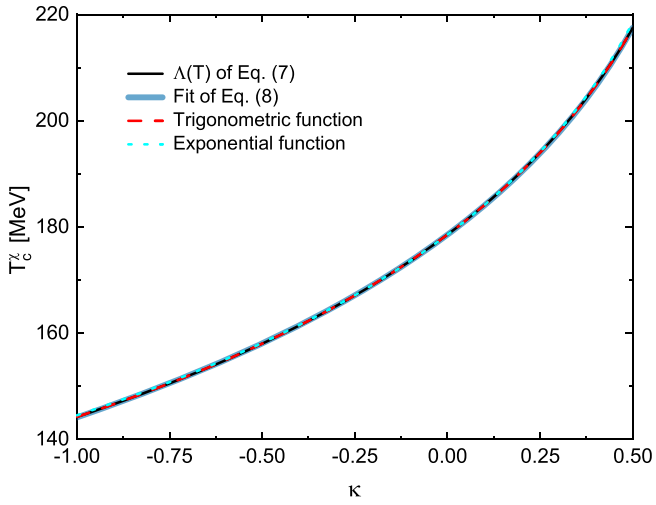

FIGURE 1 Chiral critical temperature T_c^χ, at vanishing chemical potential, as function of κ.

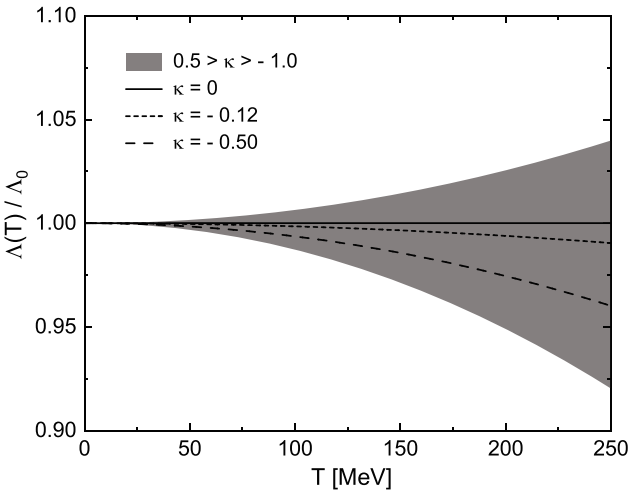

FIGURE 2 $\Lambda(T)/\Lambda_0$ as a function of the temperature for different values of κ.

trigonometric functions. We have verified that all of them lead to a similar thermal behavior for the form factor. Consequently, the chiral critical temperatures (at zero μ_B) obtained for these functional forms, as functions of κ, are almost identical. This indicates that the phenomenology predicted by the model is not sensitive to a specific temperature dependence for Λ.

In the current parameter configuration, the transition from the phase of chiral symmetry breaking to normal QM occurs as a gradual crossover. The critical temperature is determined by the peak of the chiral susceptibility, which is denoted by $-\partial\langle\bar{q}q\rangle/\partial m_c$.

In Figure 1 we plot the obtained chiral critical temperature (T_c^χ) at zero baryonic chemical potential as a function of κ for the set of parameters previously defined. It is straightforward to note the equivalence between this behavior and that obtained in Pagura et al. (2012) for the so-called Set C, which is the one where the chiral transition at $\mu_B = 0$ is always, as a function of T_0, of crossover type.

It can be easily verified that the parameterization proposed in Equation (7) as a function of κ (covering the range $-1 < \kappa < 0.5$) up to temperature values of 250 MeV, does not modify $\Lambda(T)$ by more than a 10%, and it is possible to adjust the value of the chiral critical temperature T_c^χ from 140 to almost 220 MeV. Furthermore, if we fit the critical temperature curve to a function $\kappa(T)$ of the form

$$\kappa(T) = a - e^{\frac{b-T}{c}}, \tag{8}$$

we obtain $a = 0.857 \pm 0.001$, $b = 171.66 \pm 0.05$ and $c = 44.48 \pm 0.05$. This function allows calculating κ to have the desired chiral critical temperature at zero baryonic chemical potential. In particular for κ equal to -0.12 and -0.50 we obtain the critical temperatures calculated by LQCD for SU(2) and SU(3), namely $T_c^\chi = 173$ and 158 MeV, respectively (Borsanyi et al. 2020; Karsch & Laermann 2004). This effect is illustrated in Figure 2, depicting the $\Lambda(T)/\Lambda_0$ variation with temperature. The shaded area represents the range $-1 < \kappa < 0.5$ discussed earlier. The dotted and dashed lines represent the specific values of $\kappa = -0.12$ and $\kappa = -0.50$ respectively, derived from the fitting of the critical temperatures. We observe that the ratio $\Lambda(T)/\Lambda_0$ demonstrates minimal sensitivity to low temperatures, thus preserving the entirety of the phase diagram, except for the high-temperature and low-chemical potential region. This specific area aligns with the critical temperatures predicted by LQCD, thus serving as our focal point for matching.

Finally, as depicted in Figure 3, the impact of Equation (7) on the phase diagram is shown for $\eta_D = G_D/G_S = 1.1$ and $\eta_V = G_V/G_S = 0.5$. These parameters effectively replicate the modern astrophysical data at $T = 0$, as mentioned in Contrera et al. (2022). The phase transition curves for $\kappa = 0, -0.12, -0.50$ are denoted by black, blue, and red lines, respectively. The onset of diquark condensation is minimally influenced by the value of κ. Similarly, the distinct chiral restoration curves overlap at lower temperatures. As the chemical potential decreases, however, the curves gradually separate, aligning with the values illustrated in Figure 1.

3 | ASTROPHYSICAL APPLICATIONS

We use a two-phase description to account for the transition from nuclear matter to QM in order to obtain the mass-radius relations of proto-NS or post-merger

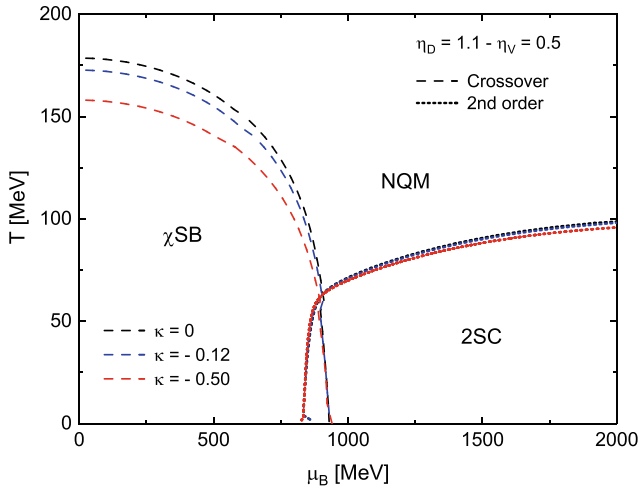

FIGURE 3 Phase diagrams for $\eta_D = 1.1$ and $\eta_V = 0.5$ with $\mu_{\nu_e} = 0$ for $\kappa = 0, -0.12, -0.5$ in black, blue and red lines, respectively.

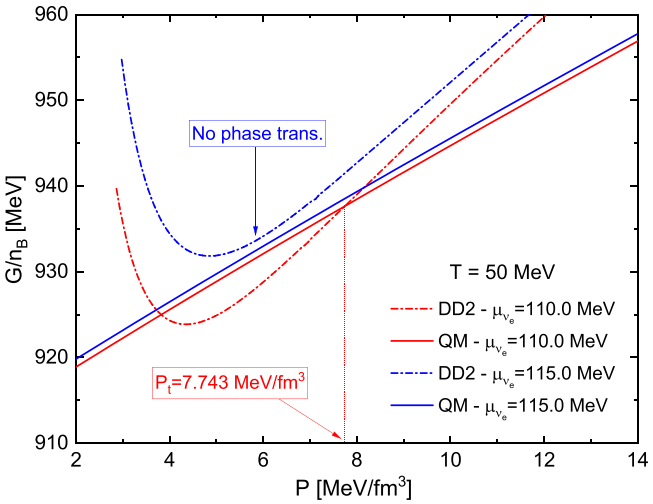

FIGURE 4 Hadron and QM EOS for $T = 50$ MeV, considering the relation $\mu_{\nu_e} = \alpha T$, with $\alpha = 2.2$ and 2.3.

objects. For QM we use the nonlocal NJL model presented above, which includes a density-dependent bag pressure and whose free parameters have been chosen to better reproduce modern astrophysical constraints. On the other hand, the interactions between baryons in the hadronic phase of nuclear matter are modeled using the density-dependent relativistic mean-field (DDRMF) Walecka model with the well-known DD2 parametrization (Malfatti et al. 2019; Typel 2018; Typel & Wolter 1999). In addition, our study incorporates a NS crust, including the Baym-Pethick-Sutherland (BPS) model (Baym et al. 1971) to characterize the hadronic EOS at densities below the nuclear saturation density.

To obtain the hadronic and QM EOS, the energy density, ϵ, is determined by the Gibbs relation:

$$\epsilon = -P + TS + \sum_j \mu_j \, n_j, \tag{9}$$

where $P = P_{q,B} + P_{lep}$, $S = \frac{\partial P}{\partial T}$ and $n_j = \frac{\partial P}{\partial \mu_j}$ (j stands for all the particles of each phase, including leptons).

The phase transition between hadronic and QM is described by a Maxwell construction, where it is required that the total pressure P and Gibbs free energy per baryon G/n_B of the two phases coincide at the phase transition point, being G the last term in Equation (9) and $n_B = \partial P/\partial \mu_B$, the number baryon density. Outside the phase transition, the phase with lower Gibbs free energy per baryon is to be chosen as the physical one. Once the pressure of the phase transition (P_t) has been found, the hybrid EOS es constructed with the energy densities corresponding to each phase.

In a NS at finite temperature, neutrinos are trapped in the stellar core. Within the scope of our analysis, we consider that the trapped neutrinos exhibit a linear temperature dependence (considering different astrophysical scenarios as in Lugones & Grunfeld 2021). In this work, this linear relation is specifically characterized by $\mu_{\nu_e} = 2.2\ T$, which constitutes the maximum possible value for μ_{ν_e} that leads to hybrid EOS at $T = 50$ MeV, as it is shown in Figure 4. Note that for the hadronic phase, at densities lower than $n_B \sim 5.10^{-2}$ fm^{-3} (corresponding to $P < 5$ MeV.fm^{-3}), G/n_B increases as n_B decreases, but the transition is considered where the crossing occurs in the positive slope region.

To rate and compare the obtained hybrid EOS with astrophysical observational constraints (Abbott & e. a 2018; Hebeler et al. 2013; Miller & e. a 2021), the Tolman-Oppenheimer-Volkoff (TOV) equations for a static nonrotating, spherical-symmetric star (Oppenheimer & Volkoff 1939; Tolman 1939) has to be solved. As can be seen in fig. 7 of Contrera et al. (2022), the corresponding EOS at $T = 0$ satisfies very well all the modern observational constraints.

In Figure 5, the mass-radius relations for the hybrid compact object configurations are presented. The density-dependent DD2 model with a BPS EOS at lower densities is used to represent the inner and outer star crusts in the hadronic phase, while the QM model described earlier stands for the inner core matter of the stars. The solid dots in the lines indicate the Hadron-to-QM onsets. Three distinct relevant temperatures are displayed, namely $T = 0, 25$ and 50 MeV in orange, green, and blue lines, respectively. Each considered value could be identified with each of the following scenarios (see Lugones & Grunfeld (2021)): (i) cold NS with extremely low temperatures and no trapped neutrinos, (ii) proto-NS with intermediate temperatures and nonzero quantity of trapped neutrinos,

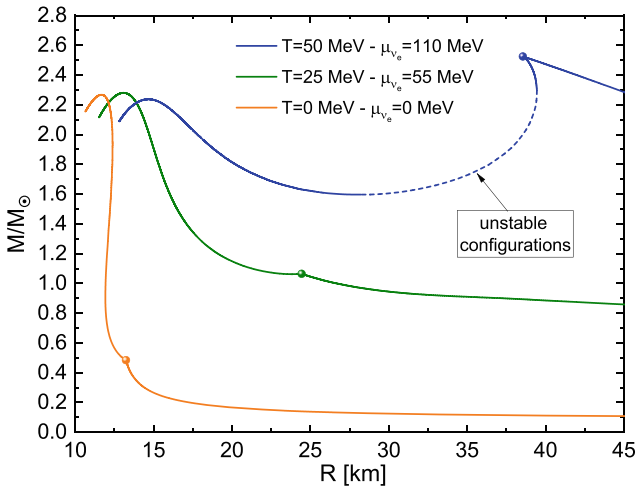

FIGURE 5 Compact hybrid object configurations for $\kappa = 0$, $\mu_{\nu_e} = 2.2\ T$, $T = 50, 25, 0$ MeV.

and (iii) post-merger object that could reach relatively high temperatures, with significant neutrino trapping amount.

Configurations featuring low radii and maximum masses are clustered around $2.3M_\odot$, indicating a slight decline with variations in T and μ_{ν_e}. However, their corresponding radii increase some kilometers with increasing temperature. In addition, it can be observed that for the highest T and μ_{ν_e} case (blue line), there is a region of unstable configurations (traced line in the plot), but two kinds of stable configurations rise in the region of remarkable high star mass and radius: with lower central densities, there is no QM in the inner core, but beyond the Hadron-QM onset (blue solid dot) there is a small region of stable configurations with QM cores and, even though, high star mass and radius values.

4 | CONCLUSIONS

In this study, we adopt a nonlocal Nambu–Jona–Lasinio (NJL) model incorporating a Gaussian form factor that depends on the spatial components of the momentum (3D-FF). Focusing on the $T - \mu_B$ plane, we explore several aspects within the phase diagram. Initially, we hypothesize that the range of interactions in momentum space may vary with temperature, enabling us to derive critical temperature values based on LQCD predictions. The impact of this assumption for $\Lambda(T)$ on the phase diagram is notably significant in the low-density and high-temperature region, aligning with expectations and corresponding to the available LQCD results. Furthermore, we integrate our QM model into a hybrid framework to examine the combined effects of temperature and neutrino trapping in compact object configurations. The hadronic phase is characterized by the DDRMF EOS with DD2 parametrization, which accounts for temperature and neutrinos trapped within the system. The model's input parameters are selected to align with contemporary multi-messenger observational data (as previously introduced in Contrera et al. (2022) at zero temperature). After conducting a thorough analysis of the QM phase diagram, considering the interplay of trapped neutrinos and temperature, we established both factors influence the diagram. Our analysis assumes a linear relationship between the neutrino chemical potential and temperature, expressed as $\mu_{\nu_e} = \alpha T$. Our findings consistently indicate the presence of hybrid configurations for temperatures up to 50 MeV. However, with a slightly higher linear relationship denoted by an increased α value, the hybrid configurations disappear, giving rise to pure hadronic stellar objects. While our results indicate that temperature and neutrinos have a negligible impact on the maximum mass of the hybrid configuration, we observe an expansion in the radius of the 'hot' compact object. Moreover, it can be noted a substantial effect in the onset of hybrid star configurations with the combined influence of temperature and trapped neutrinos. Finally, for the case of higher T and μ_{ν_e} (representing a post-merger scenario), it can be observed as a region of high mass and radius stable compact objects, with and without QM in their inner cores.

ACKNOWLEDGMENTS

This work has been partially funded by CONICET, ANPCyT, and UNLP (Argentina) under Grants No. PIP 11220210100150CO, PICT19-00792, PICT20-01847, and X960.

ORCID

G. A. Contrera https://orcid.org/0000-0002-5984-3454
A. G. Grunfeld https://orcid.org/0000-0002-6523-7469

REFERENCES

Abbott, B. P., et al. 2018, *Phys. Rev. Lett.*, *121*(16), 161101.
Abuki, H., Ciminale, M., Gatto, R., & Ruggieri, M. 2009, *Phys. Rev. D*, *79*, 034021.
Ayriyan, A., Blaschke, D., Grunfeld, A., Alvarez-Castillo, D., Grigorian, H., & Abgaryan, V. 2021, *Eur. Phys. J. A*, *57*(11), 318.
Baym, G., Pethick, C., & Sutherland, P. 1971, *Astrophys. J.*, *170*, 299.
Blanquier, E. 2017, *Eur. Phys. J. A*, *53*(6), 137.
Borsanyi, S., Fodor, Z., Guenther, J. N., et al. 2020, *Phys. Rev. Lett.*, *125*(5), 052001.
Burgio, G., Schrock, M., Reinhardt, H., & Quandt, M. 2012, *Phys. Rev. D*, *86*, 014506.
Contrera, G., Blaschke, D., Carlomagno, J. P., Grunfeld, A., & Liebing, S. 2022, *Phys. Rev. C*, *105*(4), 045808.
Diakonov, D., & Oswald, M. 2004, *Phys. Rev. D*, *70*, 105016.
Ding, H.-T., Karsch, F., & Mukherjee, S. 2015, *Int. J. Mod. Phys. E*, *24*(10), 1530007.

Fukushima, K., & Hatsuda, T. 2011, *Rept. Prog. Phys.*, *74*, 014001.
Fukushima, K., & Skokov, V. 2017, *Prog. Part. Nucl. Phys.*, *96*, 154.
Gomez Dumm, D., Blaschke, D. B., Grunfeld, A. G., & Scoccola, N. N. 2008, *Phys. Rev. D*, *78*, 114021.
Hatsuda, T., & Kunihiro, T. 1994, *Phys. Rept.*, *247*, 221.
Hebeler, K., Lattimer, J. M., Pethick, C. J., & Schwenk, A. 2013, *Astrophys. J.*, *773*, 11.
Kapusta, J. I., & Gale, C. 2011, *Finite-Temperature Field Theory: Principles and Applications*, Cambridge University Press (Cambridge, UK).
Karsch, F. 2002, *Nucl. Phys. A*, *698*, 199.
Karsch, F., & Laermann, E. 2004, in: *Quark-Gluon Plasma 3*, eds. R. C. Hwa & X.- N. Wang, World Scientific (Singapore), 1.
Klevansky, S. P. 1992, *Rev. Mod. Phys.*, *64*, 64996708.
Lattimer, J. M., & Prakash, M. 2016, *Phys. Rept.*, *621*, 127.
Lugones, G., & Grunfeld, A. G. 2021, *Phys. Rev. D*, *104*(10), L101301.
Malfatti, G., Orsaria, M. G., Contrera, G. A., Weber, F., & Ranea-Sandoval, I. F. 2019, *Phys. Rev. C*, *100*(1), 015803.
Miller, M. C., et al. 2021, *Astrophys. J. Lett*, *918*(2), L28.
Nambu, Y., & Jona-Lasinio, G. 1961a, *Phys. Rev.*, *122*, 345.
Nambu, Y., & Jona-Lasinio, G. 1961b, *Phys. Rev.*, *124*, 246.
Oppenheimer, J. R., & Volkoff, G. M. 1939, *Phys. Rev.*, *55*, 374.
Page, D., & Reddy, S. 2006, *Ann. Rev. Nucl. Part. Sci.*, *56*, 327.
Pagura, V., Gomez Dumm, D., & Scoccola, N. N. 2012, *Phys. Lett. B*, *707*, 76.
Polyakov, A. M. 1978, *Phys. Lett. B*, *72*, 477.
Roessner, S., Ratti, C., & Weise, W. 2007, *Phys. Rev. D*, *75*, 034007.
Tolman, R. C. 1939, *Phys. Rev.*, *55*, 364.
Typel, S. 2018, *Particles*, *1*(1), 2.
Typel, S., & Wolter, H. H. 1999, *Nucl. Phys.*, *A656*, 331.
Vogl, U., & Weise, W. 1991, *Prog. Part. Nucl. Phys.*, *27*, 195.

AUTHOR BIOGRAPHY

G. A. Contrera is a researcher at Instituto de Fisica La Plata (IFLP), affiliated with CONICET and the Department of Physics, Faculty of Exact Sciences, National University of La Plata (UNLP). Additionally, the author serves as an Adjunct Professor in the same Physics Department.

How to cite this article: Contrera, G. A., Carlomagno, J. P., & Grunfeld, A. G. 2023, *Astron.Nachr.*, e20230170. https://doi.org/10.1002/asna.20230170